Smart Mater. Struct. **17** (2008) 025025 (9pp) doi:10.1088/0964-1726/17/2/025025

Analysis of a nanopositioning actuator using numerical and analytic methods

Jong Seok Rho[1], Chang Hwan Lee[2], Tae-Kyung Chung[3], Chang-Hwan Im[4] and Hyun Kyo Jung[1]

[1] School of Electrical Engineering and Computer Science, Seoul National University, Kwanak-gu, Seoul, Korea
[2] Korea Electrical Engineering and Science Research Institute, Kwanak-gu, Seoul, Korea
[3] School of Electrical and Electronics Engineering, Chung Ang University, Dongjak-gu, Seoul, Korea
[4] Department of Biomedical Engineering, Yonsei University, Wonju-si, Korea

E-mail: zzong@elecmech.snu.ac.kr, lchkhk@snu.ac.kr, tkchung@cau.ac.kr, ich@yonsei.ac.kr and hkjung@snu.ac.kr

Received 28 June 2007, in final form 10 January 2008
Published 29 February 2008
Online at stacks.iop.org/SMS/17/025025

Abstract

In this paper, we report on our study of a nanopositioning actuator (NPA), which uses an impact/inchworm mechanism. Various kinds of similar precise positioning actuators, which use the same working mechanism, have been proposed by many researchers for several decades. However, characteristic analysis and design methods for the NPA have not been proposed yet. Moreover, the characteristic analysis and design methods for similar actuators were approximate and inefficient.

Hence, this paper presents an analysis method for the NPA, which is based on a combination of numerical and analytic methods, shedding light on the complex working mechanism and taking significant factors in the analysis into consideration for an exact and efficient characteristic analysis of the NPA and similar machines. In the present study, the mechanical and electrical systems of the NPA were prototyped. Finally, the effectiveness of the NPA, the feasibility of the clarified complex working mechanism, and the adequacy of the proposed analysis method were verified by experiments.

(Some figures in this article are in colour only in the electronic version)

1. Introduction

Miniaturization and high precision are becoming important trends in modern industry. These trends in turn drive the increasing demand for precise positioning actuators. As a consequence, lots of precise positioning actuators are being and have been proposed by many researchers for several decades. Since many kinds of actuators need very complex designs, high precision manufacturing, error compensators, temperature controls, and so on, most of the existing precise positioning actuators suffer from critical problems such as large size, large energy consumption, and high production/maintenance costs, and so on [1–21]. To address these problems, various kinds of precise positioning actuators based on piezoelectricity have been proposed by many researchers. The piezoelectric actuators have several advantages such as high resolution to the sub-nanometer scale, simple structure, small size, a great deal of freedom in design, and so on. Among the many kinds of piezoelectric positioning actuators, the actuators using the impact or the inchworm mechanism have the merits of being small in size, having low energy consumption, and being very economical in their production/maintenance costs [11–16]. Therefore, the NPA, which uses an impact/inchworm mechanism, was selected for study as the precise positioning actuator in our research.

There are many other kinds of precision machines, which use the same impact or inchworm mechanism as the NPA. References [1–16] discuss such machines. However, characteristic analysis and design methods for the NPA have not been proposed yet. Moreover, the characteristic analysis and design methods for similar machines were approximate and inefficient. This was because they used only a rough

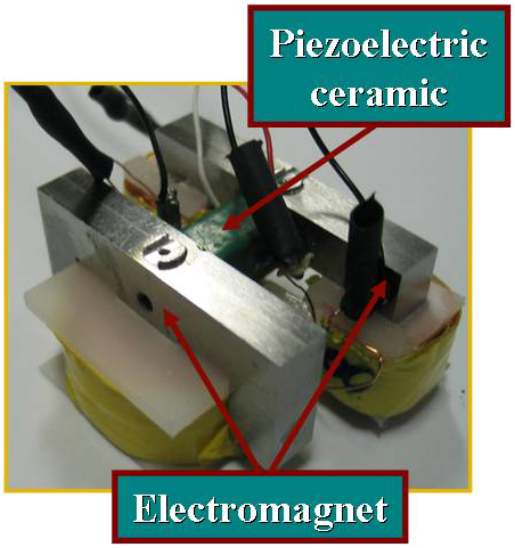

Figure 1. Prototyped NPA.

analytic method or an experimental trial-and-error method for analysis and design. These methods did not clearly articulate the complex working mechanism. They did not take significant factors into consideration in the analysis, such as the slippage, the electromagnetic force relation, the frequency dependency, and so on. References [8] and [9] suggested a characteristic analysis method for machines which use the impact/inchworm mechanism by using an approximate analytic method. However, only a rough characteristic analysis has been possible because rough analytic equations have only been used for the characteristic analysis without the consideration of the complex working mechanism and the significant factors in the analysis. For example, reference [9] mentions the need for clarifying the relationship between the electromagnetic force and slippage, but this remains an unsolved problem. In the present study, to solve this problem and to analyze exactly and efficiently the characteristics of machines which use the impact or inchworm mechanism, a numerical method combined with analytic methodology is proposed. The numerical method, 3D-FEM, is an important and frequently indispensable part of engineering analysis and design [17–19, 29]. In this paper, the mathematical model for the analysis of the piezoelectricity is derived from [22–25] for the analysis of the piezoelectric system without consideration of the impact/inchworm mechanism. The derived governing equation for the piezoelectric system is solved numerically by 3D-FEM. However, the working mechanism of the NPA is complex. Hence, the electromagnetic force is analyzed by 3D-FEM. Moreover, governing equations describing the complex working mechanism, the impact/inchworm, are suggested and solved by the analytic method. The proposed analytic method sheds light on the complex working mechanism and describes a form similar to the actual condition, considering significant factors, which have not yet been taken into account, such as the slippage, the electromagnetic force relation, the frequency dependency, and so on. In brief, the NPA, which uses an impact/inchworm mechanism, is analyzed by combining a numerical method with an analytic method.

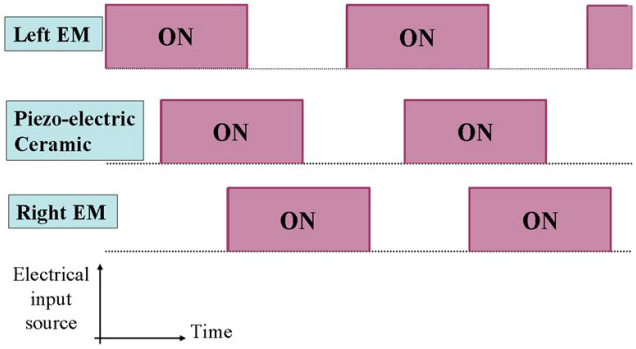

Figure 2. Wave form of the electrical input source, to the NPA.

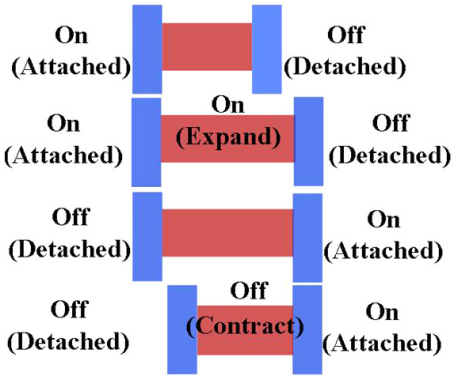

Figure 3. Ideal step motion of the NPA according to the electrical input source of figure 2.

In this research, the mechanical system and the electrical system of an NPA were prototyped. Finally, the effectiveness of an NPA in the aspects of size, cost, and so on, the reasonableness of the clarified complex working mechanism taking the significant factors into consideration in the analysis, and the adequacy of the proposed analysis method were validated by comparing their outcomes with experimental data.

2. The working principle of the NPA

Figure 1 shows the construction of the NPA. Two electromagnets (EMs) and a piezoelectric ceramic constitute the NPA. The simplified working principle is indicated in figures 2 and 3. Figure 3 is drawn only to simply explain the ideal step motion of the impact/inchworm mechanism. As shown in figure 3, the NPA moves to the right side by synchronizing three electrical input sources as indicated in figure 2. When the left EM is turned on, the left EM is attached to the bottom, which is the steel plate. At this time, the state of the right EM is off and the right EM is free to move. And then, the piezoelectric ceramic is turned on and is expanded. As a result, the right EM is slid to the right side. Maintaining the expansion of the piezoelectric ceramic, the right EM is turned on and it is attached to the bottom. At this time, the left EM is turned off and it is free to move. Then, the piezoelectric ceramic is turned off and it is contracted. Therefore, the left EM is slid to the right side. By the sequence of these synchronized actions the NPA moves

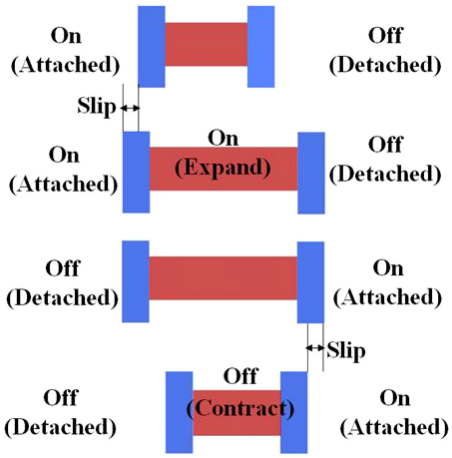

Figure 4. Real step motion of the NPA according to the electrical input source of figure 2.

to the right side, as shown in figures 2 and 3. The NPA can be moved to the left side by exchanging the right and left coil electrical input current sequences.

The working principle of the NPA is based on the inchworm principle and the impact mechanism. This means that the NPA slides by the synchronous sequence of the attaching action and the cyclic elasticity motion. The synchronous sequence of attaching by the EM and expanding and contracting by the piezoelectric ceramic is the inchworm principle. The sliding by the expansion and the contraction of the piezoelectric ceramic is the impact mechanism [1–16].

In the real case, the working condition is more complicated than the ideal condition which is shown in figure 3 and this makes the difference between the ideal case and the real one. This is because the slippage occurred as a result of the force difference in the system. In addition to the slippage, there is another condition that makes the working condition complicated and makes the difference between the real case and the ideal one. That is the different displacement of the forward electromagnet (FW-EM) and the backward electromagnet (BW-EM) due to the effect of the shape, the material, the operating frequency, and so on. The real step motion is represented in figure 4. In the real condition, the slippage has occurred and the displacements at the FW-EM and the BW-EM are different as shown in figure 4. This real step motion is different from the ideal one shown in figure 3. However, only the ideal step motion has been taken into consideration until now, although the real step motion is different from the ideal step motion, as shown in figures 3 and 4. Hence, we suggest an analysis methodology for the NPA using 3D-FEM combined with an analytic method, shedding light on the complex working mechanism and taking the significant factors into account in the analysis.

3. Prototype of the NPA

Figure 5 shows the prototype of an NPA. The important point here is that we suggest a three-contact mechanism for an NPA to reduce the manufacturing cost and to guarantee the mechanical stability of the NPA, as shown in figure 6. The NPA is controlled by the image control method using a microscope,

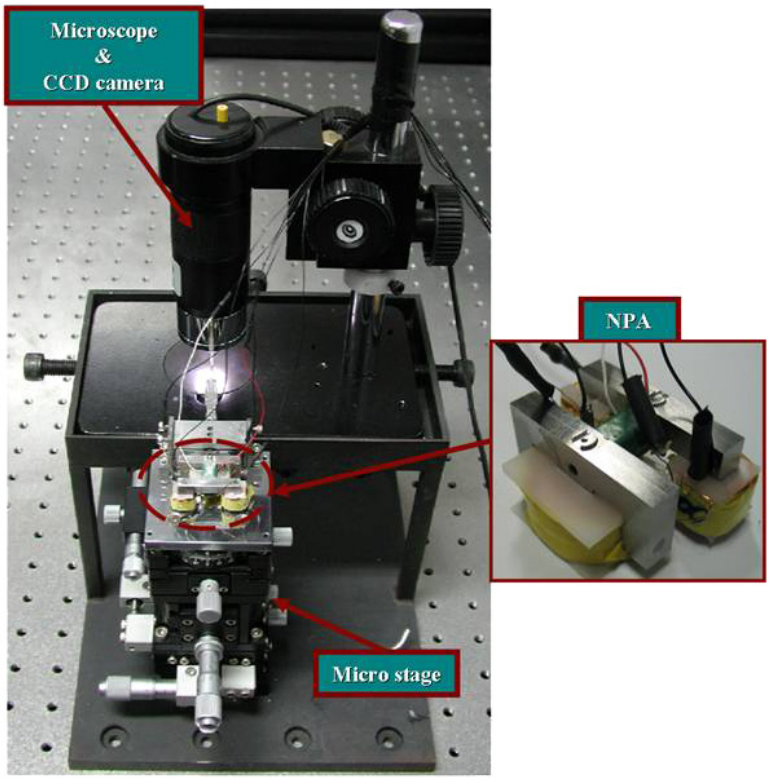

Figure 5. Prototyped mechanical system of an NPA.

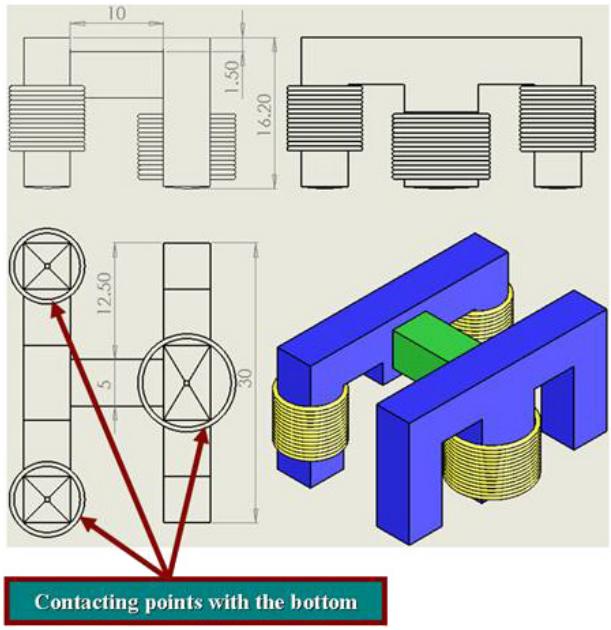

Figure 6. Indication of the contacting points, with the bottom.

a CCD camera, and a capture board. To operate the NPA, three electrical input square waves with 90° phase difference are needed, as shown in figure 2. Therefore, an SGS-THOMSON Microelectronics L297 (DIP20) Stepper Motor Controller IC, which is commonly used as a step motor driving circuit, is used for the generation of three electrical square waves with a 90° phase difference. Two waves, which have 180° phase difference, are used for the input source of the EMs. These two waves are amplified by the L298N (Multiwatt Vert.) dual full-bridge driver of the SGS-THOMSON Microelectronics device. The third wave is used for the operation of the piezoelectric ceramic with high voltage. Therefore, a half-bridge circuit with a transistor is employed to amplify the voltage.

4. Finite element formulation for the analysis of an NPA

The governing matrix equations for the numerical computation of a piezoelectric system are derived from the Hamilton variation [22–30]:

$$Mu'' + D_{uu}u' + K_{uu}u + K_{u\Phi}\Phi = F_B + F_S + F_P \quad (1)$$

$$K^t_{u\Phi}u - K_{\Phi\Phi}\Phi = Q_S + Q_P \quad (2)$$

where u, u', u'' are the mechanical displacement, velocity, and acceleration, Φ is the electrical potential, F_B, F_S, F_P are the mechanical body force, surface force, and point force, Q_S, Q_P are the electrical surface charge and the electrical point charge. M is the mass matrix, D_{uu} is the mechanical damping matrix, K_{uu} is the mechanical stiffness matrix, $K_{u\Phi}$ is the piezoelectric coupling matrix, $K_{\Phi\Phi}$ is the dielectric stiffness matrix.

The calculating algorithm for the explicit method, which includes the forward difference method, the central difference method, and so on, is simple but it has a problem in the aspect of stability. In contrast, an implicit method, such as the backward difference method, offers great advantages on the stability of the finite difference equations, since most are unconditionally stable. Therefore, a large step size in time is permitted [31]. That means that the limitation of the time step, which is a serious problem in the explicit method, is eliminated by overcoming the stability problem in the implicit method. In brief, the implicit method is unconditionally stable and more efficient in the aspect of time cost than the explicit method, so a backward difference method, which is an implicit method, is used for the analysis of the NPA in this research.

For the transient analysis of the NPA with the solution at time $t + \Delta t$, backward difference formulas with errors of the order $(\Delta t)^2$ are applied to (1) and (2). Finally, the governing equations for transient analysis of the NPA are derived:

$$M\left(\frac{-u_{t-2\Delta t} + 4u_{t-\Delta t} - 5u_t + 2u_{t+\Delta t}}{\Delta t^2}\right) + D_{uu}\left(\frac{u_{t-\Delta t} - 4u_t + 3u_{t+\Delta t}}{2\Delta t}\right) + K_{uu}u_{t+\Delta t} + K_{u\Phi}\Phi_{t+\Delta t} = F_B + F_S + F \quad (3)$$

$$K^t_{u\Phi}u_{t+\Delta t} + K_{\Phi\Phi}\Phi_{t+\Delta t} = Q_S + Q_P \quad (4)$$

where Δt is the time step.

By using (3) and (4), we developed 3D-FEM software for the transient analysis of a piezoelectric system in this research.

5. Characteristic analysis and experimental results for the NPA

In this research, significant factors, such as the slippage and the electromagnetic force relation of an NPA, are defined as *external factors* and some factors, such as the NPA system's shape, material, operating frequency, input voltage, and so on, are defined as *internal factors* of this system. This paper proposes an analysis methodology taking these significant factors in the analysis into consideration, as follows.

5.1. The calculation of the ideal displacement at each EM

The first stage for the simulation of an NPA is the calculation of an *ideal displacement* by using a transient analysis with 3D-FEM. This analysis routine takes only the internal system into consideration. Hence, the simulated displacement at this stage is called the *ideal displacement*.

Figure 7 shows the transient analysis result, obtained using 3D-FEM, of the NPA when a 50 [V]/50 [Hz] electrical source is applied to the piezoelectric ceramic. The simulated displacement in figure 7 is called the *ideal displacement* of an NPA. From this simulation routine, the *ideal displacements* of a FW-EM and a BW-EM are calculated.

The value of the calculated *ideal displacement* at the steady state of the FW-EM, $(u_F)_{ideal}$, is 829 [nm] and the BW-EM, $(u_B)_{ideal}$, is −1000 [nm]. The FW-EM and the BW-EM are displaced asymmetrically because the shape of an NPA is asymmetric. Finally, the *ideal displacement* at each FW-EM and BW-EM is calculated by transient analysis using 3D-FEM and only taking *internal factors* into consideration.

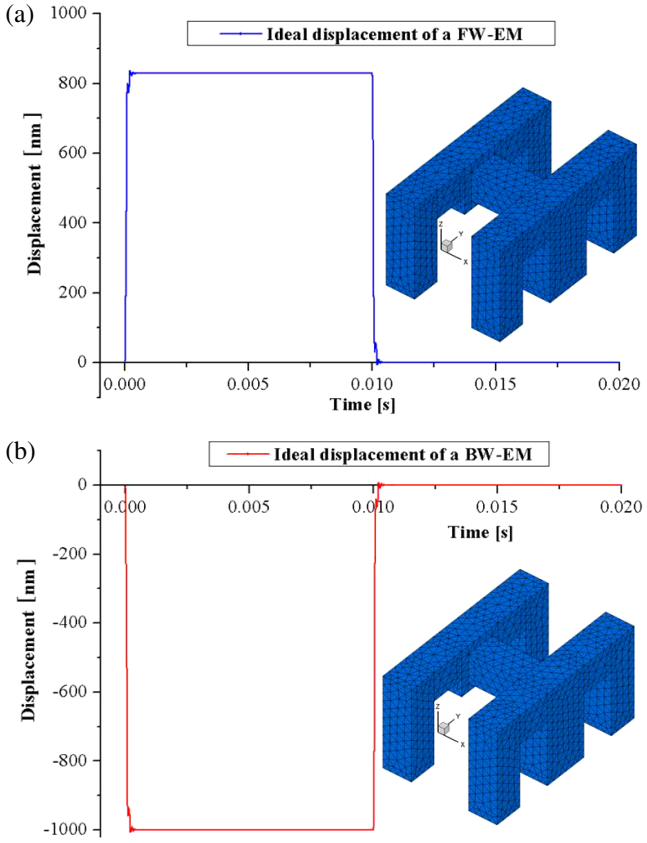

Figure 7. Simulated ideal displacement data for an NPA from 3D-FEM, when a 50 [V]/50 [Hz] electrical source is applied to a piezoelectric ceramic. (a) Simulated ideal displacement data for an FW-EM. (b) Simulated ideal displacement data for a BW-EM.

5.2. The calculation of the total displacement at each EM

The second stage for the simulation of an NPA is the calculation of a mechanical displacement of an NPA by using an analytic method taking *external factors*, such as slip losses and EM forces, into account. In our research, the NPA has been examined closely taking the complex working mechanism into consideration to calculate the *total displacement* of the NPA. The simulated final mechanical displacement, which is calculated by combining the *external factors* and the *ideal displacement* result, is called the *total displacement* in this paper. Figure 8 shows the diagram of the mechanical displacement relation in the NPA combining the *ideal displacement* and *external factors*.

From figure 8 and from the *equation of motion*, which explains the force and displacement relations [32, 33], we propose (5)–(18) for the calculation of the *total displacement* at each FW-EM and BW-EM by closely taking the complex working mechanism into consideration. The mechanical *total displacement* in the horizontal direction at each FW-EM, $(u_F)_{tot}$, and BW-EM, $(u_B)_{tot}$, can be expressed by (5)–(8) from figure 8 and the *equation of motion*. When a piezoelectric ceramic expands, the *total displacement* can be defined by (5) and (6); when it contracts, by (7) and (8):

$$(u_F)_{tot} = +(u_F)_{ideal} - (u_F)_{t.r} + (u_B)_{t.r} \quad (5)$$

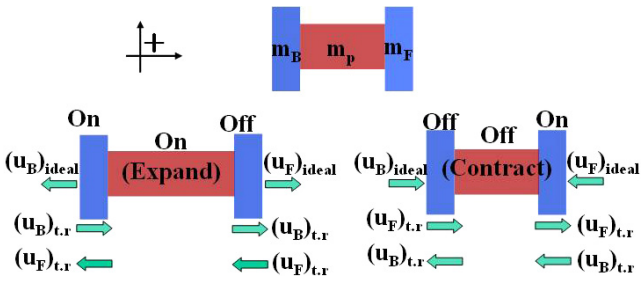

Figure 8. Diagram of the mechanical displacement relation in the NPA.

$$(u_B)_{tot} = -(u_B)_{ideal} + (u_B)_{t.r} - (u_F)_{t.r} \quad (6)$$

$$(u_F)_{tot} = -(u_F)_{ideal} + (u_F)_{t.r} - (u_B)_{t.r} \quad (7)$$

$$(u_B)_{tot} = +(u_B)_{ideal} - (u_B)_{t.r} + (u_F)_{t.r} \quad (8)$$

where $(u_F)_{t.r}$ is the mechanical displacement of the FW-EM because of the total resisting horizontal force at the FW-EM, $(u_B)_{t.r}$ is the mechanical displacement of the BW-EM because of the total resisting horizontal force at the BW-EM.

The mechanical displacement at each of the EM due to the total resisting horizontal force, $(u_F)_{t.r}$ and $(u_B)_{t.r}$, can be expressed as

$$(u_F)_{t.r} = (u_F)_{ideal} \times \frac{(F_F)_{t.r}}{(F_F)_{eff.g}}$$

$$= (u_F)_{ideal} \times \frac{(F_F)_{r.e} + (F_F)_{r.r.e} + (F_F)_{r.r}}{(m_F)_{eff} \times (a_F)_{eff}} \quad (9)$$

$$(u_B)_{t.r} = (u_B)_{ideal} \times \frac{(F_B)_{t.r}}{(F_B)_{eff.g}}$$

$$= (u_B)_{ideal} \times \frac{(F_B)_{r.e} + (F_B)_{r.r.e} + (F_B)_{r.r}}{(m_B)_{eff} \times (a_B)_{eff}} \quad (10)$$

where

$$(m_F)_{eff} = m_F + \frac{m_p}{2} \quad (11)$$

$$(m_B)_{eff} = m_B + \frac{m_p}{2} \quad (12)$$

and where $(F_F)_{t.r}$, $(F_B)_{t.r}$ are the total resisting horizontal forces at the FW-EM and the BW-EM, $(F_F)_{eff.g}$, $(F_B)_{eff.g}$ are the effective value of the generated horizontal force at the FW-EM and the BW-EM, $(F_F)_{r.e}$ is the resisting horizontal force at the FW-EM due to the EM force of a FW-EM, $(F_B)_{r.e}$ is the resisting horizontal force at the BW-EM due to the EM force of a BW-EM, $(F_F)_{r.r.e}$ is the resisting horizontal force at the FW-EM due to the residual EM force at a FW-EM, $(F_B)_{r.r.e}$ is the resisting horizontal force at the BW-EM due to the residual EM force at a BW-EM, $(F_F)_{r.r}$ is the resisting horizontal force at the FW-EM due to rest forces at a FW-EM, $(F_B)_{r.r}$ is the resisting horizontal force at the BW-EM due to rest forces at a BW-EM, $(m_F)_{eff}$, $(m_B)_{eff}$ are the effective masses of the FW-EM and the BW-EM, $(a_F)_{eff}$, $(a_B)_{eff}$ are the effective accelerations of the FW-EM and the BW-EM, m_F, m_B are the masses of the FW-EM and the BW-EM, m_P is the mass of the piezoelectric ceramic.

The effective accelerations of the FW-EM, $(a_F)_{eff}$, and the BW-EM, $(a_B)_{eff}$, are calculated by the numerical method (3D-FEM). For the calculation of the effective accelerations of the

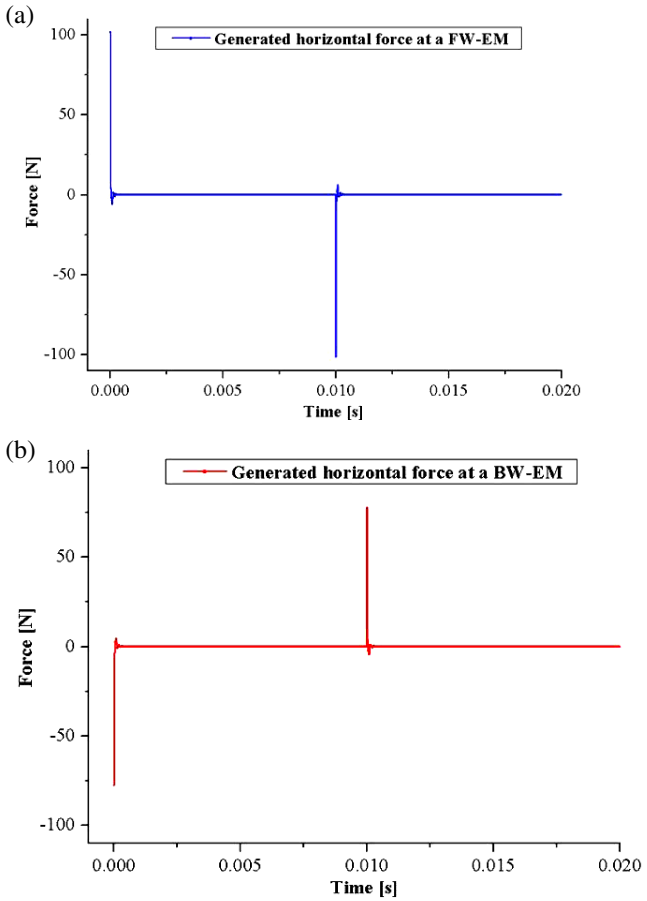

Figure 9. Calculated results for a generated horizontal force.
(a) Calculated data for a generated horizontal force at FW-EM.
(b) Calculated data for a generated horizontal force at BW-EM.

FW-EM, $(a_{\mathrm{F}})_{\mathrm{eff}}$, and the BW-EM, $(a_{\mathrm{B}})_{\mathrm{eff}}$, at time $t + \Delta t$, the backward difference formula with errors of the order $(\Delta t)^2$ is used for the derivation of the governing equations, as follows:

$$(a_{\mathrm{F}})_{\mathrm{eff}} = [-(u_{\mathrm{Fsur\_ave}})_{t-2\Delta t} + 4(u_{\mathrm{Fsur\_ave}})_{t-\Delta t} - 5(u_{\mathrm{Fsur\_ave}})_{t} + 2(u_{\mathrm{Fsur\_ave}})_{t+\Delta t}]/(\Delta t^2) \quad (13)$$

$$(a_{\mathrm{B}})_{\mathrm{eff}} = [-(u_{\mathrm{Bsur\_ave}})_{t-2\Delta t} + 4(u_{\mathrm{Bsur\_ave}})_{t-\Delta t} - 5(u_{\mathrm{Bsur\_ave}})_{t} + 2(u_{\mathrm{Bsur\_ave}})_{t+\Delta t}]/(\Delta t^2) \quad (14)$$

where $(u_{\mathrm{Fsur\_ave}})_t$, $(u_{\mathrm{Fsur\_ave}})_t$ are the averaged mechanical displacements at time t on the surfaces of the FW-EM and the BW-EM, respectively.

The ideal displacements, $(u_{\mathrm{F}})_{\mathrm{ideal}}$ and $(u_{\mathrm{B}})_{\mathrm{ideal}}$, are calculated by 3D-FEM as shown in figure 7. Also, the effective values of the generated horizontal forces, $(F_{\mathrm{F}})_{\mathrm{eff.g}}$ and $(F_{\mathrm{B}})_{\mathrm{eff.g}}$, are calculated by 3D-FEM and (9)–(14). The results are shown in figure 9. In this study, these variables are constants. This is because the input electrical source, to a piezoelectric ceramic, is fixed only at 50 [V]/50 [Hz]. The effective masses, $(m_{\mathrm{F}})_{\mathrm{eff}}$ and $(m_{\mathrm{B}})_{\mathrm{eff}}$, are also stationary. This is because the mass is not changed during the operation. The resisting horizontal force which results from the rest forces at a FW-EM, $(F_{\mathrm{F}})_{\mathrm{r.r}}$, is also a fixed variable equal to 0.01 [N]. This is because the resistance of an LM guide seal is the rest force in this research. The resisting horizontal force which results from the rest forces at a BW-EM, $(F_{\mathrm{B}})_{\mathrm{r.r}}$, is a constant equal to 0 [N]. This is because there are no rest forces. Those fixed variables are tabulated in table 1 where the signs follow the arrow directions of figure 8.

Table 1. Simulated data for fixed variables.

Variable	Value	Variable	Value
$(u_{\mathrm{F}})_{\mathrm{ideal}}$	829 [nm]	$(u_{\mathrm{B}})_{\mathrm{ideal}}$	1000 [nm]
$(m_{\mathrm{F}})_{\mathrm{eff}}$	19.7 [g]	$(m_{\mathrm{B}})_{\mathrm{eff}}$	12.5 [g]
$(F_{\mathrm{F}})_{\mathrm{eff.g}}$	72.1 [N]	$(F_{\mathrm{B}})_{\mathrm{eff.g}}$	54.9 [N]
$(F_{\mathrm{F}})_{\mathrm{r.r}}$	0.01 [N]	$(F_{\mathrm{B}})_{\mathrm{r.r}}$	0 [N]

Table 2. Simulated data for the resisting horizontal forces, which are generated due to EM forces.

Input current [A]	$(F_{\mathrm{F}})_{\mathrm{r.e}}$ [N]	$(F_{\mathrm{B}})_{\mathrm{r.e}}$ [N]	$(F_{\mathrm{F}})_{\mathrm{r.r.e}}$ [N]	$(F_{\mathrm{B}})_{\mathrm{r.r.e}}$ [N]
0.4	2.8	4.6	2.0	3.2
0.6	5.0	6.8	3.5	4.8
0.8	6.0	8.7	4.2	6.1
1.0	6.8	9.8	4.7	6.8

Resisting horizontal forces due to the EM force, $(F_{\mathrm{F}})_{\mathrm{r.e}}$ and $(F_{\mathrm{B}})_{\mathrm{r.e}}$, are calculated using (15)–(16) and 3D-FEM, using the ANSYS commercial software. The resisting horizontal forces due to the residual EM forces at a FW-EM, $(F_{\mathrm{F}})_{\mathrm{r.r.e}}$, and at a BW-EM, $(F_{\mathrm{B}})_{\mathrm{r.r.e}}$, are calculated using (17) and (18). The simulation results are tabulated in table 2.

$$(F_{\mathrm{F}})_{\mathrm{r.e}} = \mu_s \times (F_{\mathrm{F}})_{\mathrm{n.e}} \quad (15)$$

$$(F_{\mathrm{B}})_{\mathrm{r.e}} = \mu_s \times (F_{\mathrm{B}})_{\mathrm{n.e}} \quad (16)$$

$$(F_{\mathrm{F}})_{\mathrm{r.r.e}} = \mu_s \times (F_{\mathrm{F}})_{\mathrm{n.r.e}} \quad (17)$$

$$(F_{\mathrm{B}})_{\mathrm{r.r.e}} = \mu_s \times (F_{\mathrm{B}})_{\mathrm{n.r.e}} \quad (18)$$

where μ_{s} is the static frictional coefficient (0.17), $(F_{\mathrm{F}})_{\mathrm{n.e}}$, $(F_{\mathrm{B}})_{\mathrm{n.e}}$ are the normal EM forces at the FW-EM and at the BW-EM, $(F_{\mathrm{F}})_{\mathrm{n.r.e}}$, $(F_{\mathrm{B}})_{\mathrm{n.r.e}}$ are the normal residual EM forces at the FW-EM and at the BW-EM.

The simulated results for mechanical displacements in the horizontal direction are tabulated in table 3 with the varying input electrical source, to an EM. The signs of the listed values follow the arrow directions of figure 8.

5.3. The calculation of one cycle of displacement at each EM

By applying (9)–(18) to (5)–(8), the *total displacements* in the horizontal direction of the FW-EM, $(u_{\mathrm{F}})_{\mathrm{tot}}$, and BW-EM, $(u_{\mathrm{B}})_{\mathrm{tot}}$, can be calculated about one cycle taking significant factors into consideration. The *total displacement* about one cycle has the same meaning as the resolution of an NPA. Hence, (19) and (20) are proposed in this research for the calculation of one cycle of mechanical *total displacement* of the FW-EM, $(u_{\mathrm{F}})_{\mathrm{one\_cyc}}$, and the BW-EM, $(u_{\mathrm{B}})_{\mathrm{one\_cyct}}$. From these results, the resolution of an NPA can be simulated.

$$(u_{\mathrm{F}})_{\mathrm{one\_cyc}} = (u_{\mathrm{F}})_{\mathrm{tot\_exp}} + (u_{\mathrm{F}})_{\mathrm{tot\_con}} \quad (19)$$

$$(u_{\mathrm{B}})_{\mathrm{one\_cyc}} = (u_{\mathrm{B}})_{\mathrm{tot\_exp}} + (u_{\mathrm{B}})_{\mathrm{tot\_con}} \quad (20)$$

where $(u_{\mathrm{F}})_{\mathrm{tot\_exp}}$ is the total displacement in the horizontal direction of the FW-EM when the piezoelectric ceramic

Table 3. Simulation results for mechanical displacements in the horizontal direction about the varying input electrical source, to the EM.

		When PZT expands and BW-EM is turned on		When PZT contracts and FW-EM is turned on	
		At a FW-EM	At a BW-EM	At a FW-EM	At a BW-EM
0.4 [A]	$(u_F)_{t.r}$ [nm]	23	23	32	32
	$(u_B)_{t.r}$ [nm]	84	84	59	59
	$(u_F)_{tot}$ [nm]	891	—	−856	—
	$(u_B)_{tot}$ [nm]	—	−938	—	973
0.6 [A]	$(u_F)_{t.r}$ [nm]	41	41	58	58
	$(u_B)_{t.r}$ [nm]	124	124	87	87
	$(u_F)_{tot}$ [nm]	913	—	−858	—
	$(u_B)_{tot}$ [nm]	—	−916	—	971
0.8 [A]	$(u_F)_{t.r}$ [nm]	49	49	69	69
	$(u_B)_{t.r}$ [nm]	159	159	111	111
	$(u_F)_{tot}$ [nm]	940	—	−871	—
	$(u_B)_{tot}$ [nm]	—	−889	—	958
1.0 [A]	$(u_F)_{t.r}$ [nm]	55	55	78	78
	$(u_B)_{t.r}$ [nm]	178	178	125	125
	$(u_F)_{tot}$ [nm]	952	—	−876	—
	$(u_B)_{tot}$ [nm]	—	−877	—	953

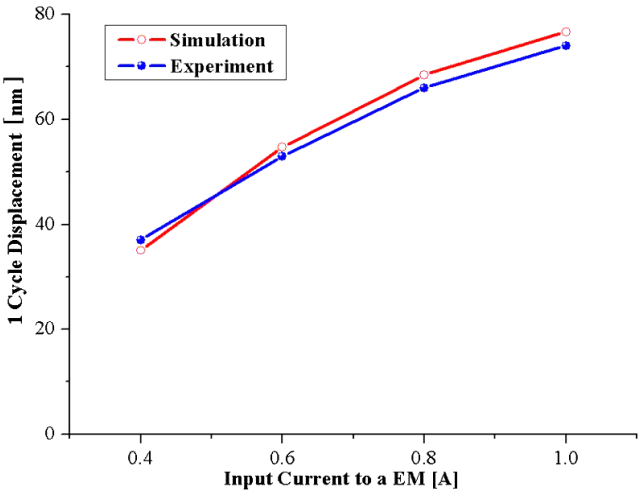

Figure 10. One cycle of displacement obtained from the simulation and the experiment, according to the varying input current, to the EM.

Table 4. One cycle of displacement obtained from the simulation and the experiment, when varying the input current, to the EM.

Input current [A]	Simulated data [nm]	Experiment data [nm]	Error [%]
0.4	35	37	5.4
0.6	55	53	3.2
0.8	69	66	3.8
1.0	77	74	3.6

expands, $(u_F)_{tot\_con}$ is the total displacement in the horizontal direction of the FW-EM when the piezoelectric ceramic contracts, $(u_B)_{tot\_exp}$ is the total displacement in the horizontal direction of the BW-EM when the piezoelectric ceramic expands, $(u_B)_{tot\_con}$ is the total displacement in the horizontal direction of the BW-EM when the piezoelectric ceramic contracts.

Finally, one mechanical cycle of displacement, in other words the resolution, of an NPA is calculated by using (19) and (20) and table 3. The simulated data and the experimental data for the one cycle of *total displacement* are shown in figure 10 and table 4 with varying input electrical source of the EM. The result of the simulation, which has been calculated by the proposed method, fitted with the experimental data. This good agreement is induced by selecting the static frictional coefficient as 0.17, although the experimental value of the static frictional coefficient is about 0.15–0.2. This variation of the static frictional coefficient value caused some error between the experimental data and simulation ones. But those errors were in an acceptable range and the data patterns were the same. Hence, we selected the static frictional coefficient at 0.17 in order to show the good agreement with the experimental data. This proved that the explained complex working mechanism, which is the impact and inchworm one, taking the *internal* and the *external factors* into account, is correct and the proposed analysis methodology is reasonable. Therefore, it may be applicable to many other kinds of actuators which use similar working mechanisms.

6. Conclusion

In the present paper, an analysis methodology for the NPA is proposed and described, which is based on 3D-FEM combined with an analytic method, shedding light on the complex working mechanism and taking significant factors, which have not yet been considered, into consideration for the exact and efficient characteristic analysis of the NPA and similar machines.

For the verification of this research, a mechanical system and an electrical system of an NPA have been prototyped. Finally, the effectiveness of an NPA, the reasonableness of a clarified complex working mechanism, and the adequacy of the proposed analysis method have been validated by comparing these outcomes with experimental data.

Acknowledgments

This research was performed for ‘The Development of The Linear Motor for Precision Positioning’, funded by the

Sam-Hwa-Yang-Heng Co. Ltd, PALABS Co. Ltd, and Dong-Il Tech Co. Ltd.

Appendix

NEC/TOKIN AE0505D08 (x-axis poling material) is used as a piezoelectric material, as follows:

Mechanical stiffness matrix for constant electric field E:

$$c^{\mathrm{E}} = \begin{bmatrix} 8.957 & 5.356 & 5.356 & 0.0 & 0.0 & 0.0 \\ 5.356 & 10.87 & 5.845 & 0.0 & 0.0 & 0.0 \\ 5.356 & 5.845 & 10.87 & 0.0 & 0.0 & 0.0 \\ 0.0 & 0.0 & 0.0 & 2.513 & 0.0 & 0.0 \\ 0.0 & 0.0 & 0.0 & 0.0 & 2.227 & 0.0 \\ 0.0 & 0.0 & 0.0 & 0.0 & 0.0 & 2.227 \end{bmatrix} \times 10^{10}\ [\mathrm{N\,m^{-2}}].$$

Piezoelectric matrix:

$$e = \begin{bmatrix} 26.136 & -13.96 & -13.96 & 0.0 & 0.0 & 0.0 \\ 0.0 & 0.0 & 0.0 & 0.0 & 0.0 & 20.713 \\ 0.0 & 0.0 & 0.0 & 0.0 & 20.713 & 0.0 \end{bmatrix} [\mathrm{C\,m^{-2}}].$$

Permittivity matrix for a constant mechanical strain S:

$$\varepsilon^{\mathrm{S}} = \begin{bmatrix} 25.888 & 0.0 & 0.0 \\ 0.0 & 25.007 & 0.0 \\ 0.0 & 0.0 & 25.007 \end{bmatrix} \times 10^{-9}\ [\mathrm{F\,m^{-2}}].$$

Density: $\rho = 8000\ [\mathrm{kg\,m^{-3}}]$; mechanical quality factor: $Q = 70$.

M19-steel is used for an EM, as follows:

Mechanical stiffness matrix:

$$c_{\mathrm{m}} = \begin{bmatrix} 262.5 & 112.5 & 112.5 & 0.0 & 0.0 & 0.0 \\ 112.5 & 262.5 & 112.5 & 0.0 & 0.0 & 0.0 \\ 112.5 & 112.5 & 262.5 & 0.0 & 0.0 & 0.0 \\ 0.0 & 0.0 & 0.0 & 75.0 & 0.0 & 0.0 \\ 0.0 & 0.0 & 0.0 & 0.0 & 75.0 & 0.0 \\ 0.0 & 0.0 & 0.0 & 0.0 & 0.0 & 75.0 \end{bmatrix} \times 10^{9}\ [\mathrm{N\,m^{-2}}].$$

Density: $\rho_{\mathrm{m}} = 7850\ [\mathrm{kg\,m^{-3}}]$; mechanical quality factor: $Q_{\mathrm{m}} = 3000$.

References

[1] Uchino K and Giniwicz J R 2002 *Micromechatronics* (New York: Dekker) chapter 6

[2] Uchino K 1997 *Piezoelectric Actuator and Ultrasonic Motors* (Dordrecht: Kluwer–Academic)

[3] Uchino K 1999 Recent trend of piezoelectric actuator developments micromechatronics and human science *Proc. Micromechatronics and Human Science 1999 Int. Symp. (Nov.)* pp 3–9

[4] Uchino K 1994 Piezoelectric actuators/ultrasonic motors—their developments and markets *Proc. 9th IEEE Int. Symp. on Applications of Ferroelectrics (Aug.)* pp 319–24

[5] Koc B, Cagatay S and Uchino K 2002 A piezoelectric motor using two orthogonal bending modes of a hollow cylinder ultrasonics *IEEE Transactions on Ferroelectrics and Frequency Control (April)* vol 49, pp 495–500

[6] Sashida T and Kenjo T 1993 *An Introduction to Ultrasonic Motors* (Oxford: Clarendon)

[7] Ueha S, Tomikawa Y, Kurosawa M and Nakamura N 1993 *Ultrasonic Motors: Theory and Applications* (Oxford: Clarendon) chapter 5

[8] Ikuta K, Aritomi S and Kabashima T 1992 Tiny silent linear cybernetic actuator driven by piezoelectric device with electromagnetic clamp *MEMS '92: Proc. Micro Electro Mechanical Systems, An Investigation of Micro Structures, Sensors, Actuators, Machines and Robot* (Piscataway, NJ: IEEE)

[9] Torii A, Kato H and Ueda A 2001 A miniature actuator with electromagnetic elements *Electr. Eng. Japan* **134** 70–5

[10] Furutani K, Furuichi M and Mohri N 2001 Coarse motion of 'seal mechanism' with three degrees of freedom by using difference of frictional force *Meas. Sci. Technol.* **12** 2147–53

[11] Aoyama H and Hayashi A 1999 Multiple micro robots for desktop precise production *Proc. 1st Conf. EUSPEN (Bremen)* pp 60–3

[12] Aoyama H *et al* 1999 *Proc. 14th ASPE Ann. Mtg (Monterey, CA)* pp 283–6

[13] Fuchiwaki O and Aoyama H 2002 Micromanipulation by miniature robots in a SEM vacuum chamber *J. Robot. Mechatron.* **14** 221–6

[14] Aoyama H and Fuchiwaki O 2001 Flexible micro-processing by multiple micro robots in SEM *Proc. 2001 IEEE Int. Conf. on Robotics and Automation (Seoul, May)* pp 21–6

[15] Higuchi T, Yamagata Y, Furutani K and Kudoh K 1990 Precise positioning mechanism utilizing rapid deformations of piezoelectric elements *IEEE Micro Electro Mech. Syst.* pp 222–6

[16] Ohmichi O, Yamagata Y and Higuchi T 1997 Micro impact drive mechanisms using optically excited thermal expansion *IEEE Trans. Microelectromech. Syst.* **6** 200–7

[17] Rho J-S, Joo H-W, Lee C-H and Jung H-K 2003 Analysis of ultrasonic linear motor using the finite element method and equivalent circuit *B: KIEE Int. Trans. Electr. Mach. Energy Convers. Syst.* **3-B** 159–64

[18] Kim B-J, Rho J-S and Jung H-K 2005 Optimal design of piezoelectric cantilever fan by three-dimensional finite element analysis *B: KIEE Int. Trans. Electr. Mach. Energy Convers. Syst.* **5-B** 90–4

[19] Bathe K-J 1996 *Finite Element Procedures* (Englewood Cliffs, NJ: Prentice-Hall)

[20] Lim K-J, Park S-H, Yun Y-J, Park C-H, Kang S-H and Lee J-S 2006 Characteristics of π-shaped ultrasonic motor *KIEE, J. Electr. Eng. Technol. 6* **1** 241–5

[21] Lim K-J, Park S-H, Yun Y-J, Lee K-Y, Kang S-H, Lee J-S and Jeong S-H 2006 Characteristics of disk-type linear ultrasonic motor for application to x–y stage *KIEE, J. Electr. Eng. Technol. 3* **1** 101–5

[22] Rho J-S, Kim B-J, Lee C-H, Joo H-W and Jung H-K 2005 Design and characteristic analysis of L1B4 ultrasonic motor considering contact mechanism *IEEE Trans. Ultrason. Ferroelectr. Freq. Control* **52** 2054–64

[23] Lerch R 1990 Simulation of piezoelectric devices by two- and three dimensional finite elements *IEEE Trans. Ultrason. Ferroelectr. Freq. Control* **37** 233–47

[24] Lerch R 1988 Finite element analysis of piezoelectric transducers *Proc. Ultrasonics Symp. (Oct.)* vol 2 (Piscataway, NJ: IEEE) pp 643–54

[25] Lerch R and Kaarmann H 1987 Three-dimensional finite element analysis of piezoelectric media *IEEE Ultrasonics Symp.* (Piscataway, NJ: IEEE) pp 853–8

[26] Korn A and Korn T M 1968 *Mathematical Handbook for Scientists and Engineers* (New York: McGraw-Hill)

[27] Tiersten H F 1967 Hamilton's principle for linear piezoelectric media *Proc. IEEE* **55** 1523–4

[28] Allik H and Hughes T J R 1970 Finite element method for piezoelectric vibration *Int. J. Numer. Methods Eng.* **2** 151–7
[29] Bathe K J and Wilson E 1976 *Numerical Method in Finite Element Analysis* (Englewood Cliffs, NJ: Prentice-Hall)
[30] Kagawa Y, Tsuchiya T, Kataoka T, Yamabuchi T and Furukawa T 1996 Finite element simulation of dynamic response of piezoelectric actuator *J. Sound Vib.* **191** 519–38
[31] Hoffmann K A and Chiang S T 1993 *Computational Fluid Dynamics for Engineers* vol 1 (Wichita, KS: Engineering Education System)
[32] Rao S S 1995 *Mechanical Vibrations* 3rd edn (Reading, MA: Addison-Wesley)
[33] Inman D J 1994 *Engineering Vibration* (Englewood Cliffs, NJ: Prentice-Hall)